Backscatter Modulation Design for Symbiotic Radio Networks

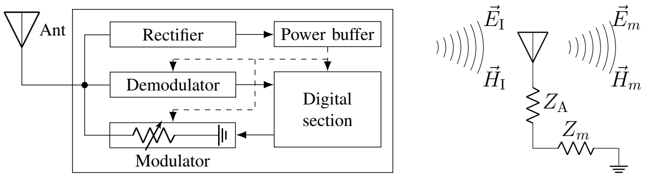

(a) Block diagram of a passive tag (b) Backscatter modualtion

Fig. 1. For a passive tag, the rectifier and demodulator rely on the incident electromagnetic wave for energy harvesting and source decoding, while the load-switcher adjusts the reradiated signal for backscatter modulation.

I. Backscatter Model

A. Backscatter Principles

A bistatic backscatter system consists of an excitation source, multiple (semi-)passive tags, and a backscatter reader. When illuminated, the tags simultaneously harvest energy, backscatter message, and demodulate the source signal if necessary. Fig. 1(a) shows a typical passive with a scattering antenna, an energy harvester, an integrated receiver[1], a load-switching modulator, and on-chip components (e.g., micro-controller, memory, and sensors). A portion of the impinging signal is absorbed by the tag while the remaining is backscattered to the space. According to Green's decomposition [2], the backscattered signal can be decomposed into the *structural mode* component and the *antenna mode* component. The former is fixed and depends on the antenna geometry and material properties[2], while the latter is adjustable and depends on the mismatch of the antenna and load impedance. Fig. 1(b) illustrates a simplified circuit and backscatter model at tag state m. The corresponding reflection coefficient is defined as[3]

$$\Gamma_m = \frac{Z_m - Z_\mathrm{A}^*}{Z_m + Z_\mathrm{A}}, \tag{1}$$

where Z_m is the load impedance at state m and Z_A is the antenna input impedance.

B. Backscatter Modulation

Backscatter modulation is achieved by switching the tag load impedance between different states. For an M-ary Quadrature Amplitude Modulation (QAM) at state $m \in \mathcal{M} \triangleq \{1, \ldots, M\}$, the reflection coefficient Γ_m maps to the signal constellation point $\bar{c}_m$ as [5]

$$\Gamma_m = \alpha \frac{\bar{c}_m}{\max_{m'} |\bar{c}_{m'}|}, \tag{2}$$

where $\alpha \in [0, 1]$ is the reflection efficiency at a given direction. For simplicity, we consider an M-ary Phase Shift Keying (PSK) with constellation set $\mathcal{C} \triangleq \{\bar{c}_1, \ldots, \bar{c}_M\}$, where the m-th constellation point is

$$\bar{c}_m = \exp\left(j \frac{2\pi m}{M}\right). \tag{3}$$

Remark 1. *For passive tags, the reflection efficiency α controls the tradeoff between the harvestable power and backscatter strength: $\alpha = 0$ corresponds to maximum power transfer to the tag, while $\alpha = 1$ with M-PSK corresponds to ideal Intelligent Reflecting Surface (IRS) with M discrete states.*

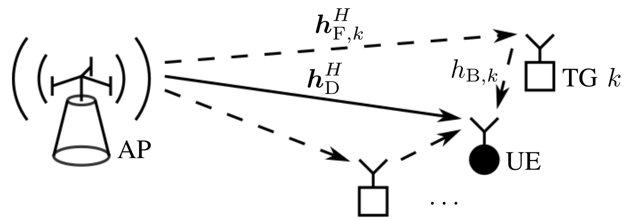

Fig. 2. A single-user multi-tag symbiotic radio system.

II. The Multi-Tag Case

A. System Model

As shown in Fig. 2, we propose a single-user (UE) multi-tag (TG) symbiotic radio network where the RF signal generated by the Q-antenna Access Point (AP) is shared by two coexisting systems. In the primary downlink system, the AP transmits information to the single-antenna user. In the secondary backscatter system, the AP acts as the carrier emitter, the K nearby single-antenna tags modulate their information over the reradiated RF signals, and the user serves as the multi-tag backscatter reader. Denote the AP-UE direct channel as $\boldsymbol{h}_\mathrm{D}^H \in \mathbb{C}^{1\times Q}$, the AP-TG $k \in \mathcal{K} \triangleq \{1, \ldots, K\}$ forward channel as $\boldsymbol{h}_{\mathrm{F},k}^H \in \mathbb{C}^{1\times Q}$, the TG k-UE backward channel as $h_{\mathrm{B},k}$, and the cascaded forward-backward channel of tag k as $\boldsymbol{h}_{\mathrm{C},k}^H \triangleq h_{\mathrm{B},k} \boldsymbol{h}_{\mathrm{F},k}^H \in \mathbb{C}^{1\times Q}$. For simplicity, we consider a quasi-static block fading model where the channel coefficients remain constant within each coherence interval and vary independently over different coherence intervals, and assume the coherence interval T is much longer than the backscatter symbol period T_c and primary symbol period T_s. We also assume the direct channel and all cascaded channels can be successfully estimated

[1]For example, [1] prototyped a compact-size pulse position demodulator based on an envelope detector, which brings great potential to coordination, synchronization, and reflection pattern control.

[2]The structural mode component can be regarded as part of the environment multipath and modeled by channel estimation [3].

[3]We assume the linear backscatter model where the reflection coefficient is irrelevant to the incident electromagnetic field at the tag [4].

and fed back to the AP.[4] Since the tags need to physically switch the loads for backscatter modulation, they communicate at a much longer symbol period (and lower rates) than the primary system. As such, we assume the transitions of all tags are perfectly synchronized, and the backscatter symbol period satisfies $T_c = NT_s$ where $N \gg 1$ is a positive integer.

Without loss of generality, we focus on the transmissions and detections during one particular backscatter symbol period. To provide a preliminary insight, we assume the primary symbol $s[n]$ at block $n \in \mathcal{N} \triangleq \{1, \ldots, N\}$ is in standard CSCG distribution, and the backscatter symbol c_k of tag k employs M-PSK modulation by (3), i.e., $c_k \in \mathcal{C}$, $\forall k \in \mathcal{K}$. Thus, the signal received by the user at block n can be expressed as[5]

$$y[n] = \left(\boldsymbol{h}_{\mathrm{D}}^H + \sum_{k \in \mathcal{K}} \sqrt{\alpha_k} \boldsymbol{h}_{\mathrm{C},k}^H c_k \right) \boldsymbol{w} s[n] + w[n], \tag{4}$$

where $\boldsymbol{w} \in \mathbb{C}^{Q \times 1}$ is the active precoder satisfying $\|\boldsymbol{w}\|^2 \leq P$, P is the average transmit power constraint at the AP, and $w[n] \sim \mathcal{CN}(0, \sigma_w^2)$ is the equivalent Additive White Gaussian Noise (AWGN) at block n. Besides, we collect the backscatter symbols of K tags into $c_{\mathcal{K}} \triangleq \{c_k : k \in \mathcal{K}\}$, stack the received signal over N blocks as $\boldsymbol{y} \triangleq [y[1], \ldots, y[N]]^T \in \mathbb{C}^{N \times 1}$, and define the equivalent channel for primary transmission as

$$\boldsymbol{h}_{\mathrm{E}}^H(c_{\mathcal{K}}) \triangleq \boldsymbol{h}_{\mathrm{D}}^H + \sum_{k \in \mathcal{K}} \sqrt{\alpha_k} \boldsymbol{h}_{\mathrm{C},k}^H c_k. \tag{5}$$

Remark 2. *The proposed symbiotic radio system includes a multiplicative Multiple Access Channel (MAC) where the AP and the tags simultaneously transmit to the user. It inspired [TODO] to perform Successive Interference Cancellation (SIC) that first non-coherently detects the primary message under backscatter uncertainty, then cancels its contribution and decodes the tag messages. This scheme requires non-coherent coding at the AP and K re-encoding, precoding, and subtraction operations at the user. However, different from the conventional MAC with Superposition Coding (SC), the symbiotic radio system involves Multiplication Coding (MC) that combines the primary and secondary messages by multiplication. Hence, novel multi-stream detection techniques should be tailored to symbiotic radio systems to accommodate the massive connectivity of tags and the multiplicative combination of links.*

B. Backscatter Detection

To reveal the impact of backscatter modulation on the primary transmission and avoid the exponential complexity of joint detection, we extend the non-coherent Ambient Backscatter Communications (AmBC) detection [11] to the multi-tag case, and propose a low-complexity energy detection to decode the backscatter symbols under primary source uncertainty. It requires no dedicated receivers or non-coherent codes at the AP, and can be readily implemented over legacy downlink systems.

Remark 3. *One key property of symbiotic radio is the primary message propagates to the user from a known channel and multiple multiplicative channels with uncertainty introduced by backscatter modulation. As such, each reflection coefficient simultaneously encodes the tag message and influences the equivalent channel of the primary link. If the backscatter symbols can be successfully decoded first, they can be modeled within the equivalent channel* (5) *as in channel training, instead of being removed by SIC.*

To explicitly specify each backscatter symbol combination, we label it by the corresponding modulation index set. For tag k at state $m_k \in \mathcal{M}$, $\forall k \in \mathcal{K}$, we define the modulation index set as $m_{\mathcal{K}} \triangleq \{m_k : k \in \mathcal{K}\}$ and the tag input combination as $\bar{c}_{m_{\mathcal{K}}} \triangleq \{\bar{c}_{m_k} : k \in \mathcal{K}\}$. Since any $\bar{c}_{m_{\mathcal{K}}}$ remains constant per N primary symbols, the received signal at block n is only subject to the variation of the primary source $s[n]$ and AWGN $w[n]$, and thus follows CSCG distribution $y_{m_{\mathcal{K}}}[n] \sim \mathcal{CN}\left(0, \sigma_{m_{\mathcal{K}}}^2\right)$ with variance

$$\sigma_{m_{\mathcal{K}}}^2 = \Bigg| \underbrace{\left(\boldsymbol{h}_{\mathrm{D}}^H + \sum_{k \in \mathcal{K}} \sqrt{\alpha_k} \boldsymbol{h}_{\mathrm{C},k}^H \bar{c}_{m_k} \right) \boldsymbol{w}}_{\boldsymbol{h}_{\mathrm{E}}^H(\bar{c}_{m_{\mathcal{K}}})} \Bigg|^2 + \sigma_w^2, \tag{6}$$

which denotes the expectation of the received power per primary block under tag modulation index set $m_{\mathcal{K}}$. For the ease of exposition, we denote the hypothesis that the tag input combination at status $i \in \mathcal{M}^{\mathcal{K}} \triangleq \{1, \ldots, M^K\}$ as $\mathcal{H}_i$, sort $\{\sigma_{m_{\mathcal{K}}}^2\}$ in ascending order by a one-to-one mapping $m_{\mathcal{K}} \mapsto i$,[6] define the received signal energy over N primary blocks as $z \triangleq \|\boldsymbol{y}\|^2$, and let $f(z \mid \mathcal{H}_i)$ be the conditional probability density function of receiving z under hypothesis $\mathcal{H}_i$. Correspondingly, z is the sum of N i.i.d. exponential variables each with mean σ_i^2, and the conditional probability density function follows Erlang distribution with shape N and scale σ_i^2 as

$$f(z \mid \mathcal{H}_i) = \frac{z^{N-1} e^{-z/\sigma_i^2}}{\sigma_i^{2N} (N-1)!}. \tag{7}$$

Remark 4. *The backscatter links essentially form a discrete-input continuous-output memoryless channel. To further reduce decoding complexity, we apply hard-decision detection and construct a Discrete Memoryless Thresholding Channel (DMTC), whose capacity is a function of both input distribution and decision thresholds [12].*

Denote the decision region of hypothesis $\mathcal{H}_i$ as

$$\mathcal{R}_i \triangleq [T_{i-1,i}, T_{i,i+1}), \tag{8}$$

where $T_{i-1,i}$ is the decision threshold between $\mathcal{H}_{i-1}$ and $\mathcal{H}_i$, and $T_{i,i+1}$ is the decision threshold between $\mathcal{H}_i$ and $\mathcal{H}_{i+1}$. We also define $T_{0,1} \triangleq 0$, $T_{M^K, M^K+1} \triangleq \infty$, and $\mathcal{T} \triangleq \{T_{0,1}, \ldots, T_{M^K, M^K+1}\}$.

[4] Due to the lack of RF chains at the passive tag, accurate and efficient Channel State Information at the Transmitter (CSIT) acquisition can be challenging. One possible approach is that the AP sends pre-defined pilots, the tags respond in well-designed manners, and the user performs least-square estimation with feedbacks [6]–[8].

[5] We omit the signal reflected by two or more times [9] and assume the time difference of arrival from different paths are negligible [10].

[6] When more than one modulation index sets yield the same energy level, the mapping is not unique and the detection fails to separate them. This blind spot issue can be mitigated by multi-antenna techniques.

Consider the Maximum-Likelihood (ML) detector for example. The likelihood ratio between hypotheses $\mathcal{H}_i$ and $\mathcal{H}_{i'}$ is [11]

$$\Lambda_{i,i'}^{\mathrm{ML}}(z) = \frac{f(z \mid \mathcal{H}_i)}{f(z \mid \mathcal{H}_{i'})} = \left(\frac{\sigma_{i'}^2}{\sigma_i^2}\right)^N \exp\left(\frac{\sigma_i^2 - \sigma_{i'}^2}{\sigma_i^2 \sigma_{i'}^2} z\right), \quad (9)$$

and the corresponding decision rule is

$$\Lambda_{i,i'}^{\mathrm{ML}}(z) \underset{\mathcal{H}_{i'}}{\overset{\mathcal{H}_i}{\lessgtr}} 1 \iff z \underset{\mathcal{H}_{i'}}{\overset{\mathcal{H}_i}{\lessgtr}} T_{i,i'}^{\mathrm{ML}}, \quad (10)$$

where the detection threshold between $\mathcal{H}_i$ and $\mathcal{H}_{i'}$ is

$$T_{i,i'}^{\mathrm{ML}} \triangleq N \frac{\sigma_i^2 \sigma_{i'}^2}{\sigma_i^2 - \sigma_{i'}^2} \log \frac{\sigma_i^2}{\sigma_{i'}^2}. \quad (11)$$

Remark 5. *Although the ML decision threshold is optimal in terms of the likelihood function, it is not necessarily capacity-achieving, although the performance gap can be negligible in the single-tag BIBO case.*

Once the decision region is determined, we can formulate an equivalent point-to-point DMC from tag input combination alphabet $\mathcal{M}^{\mathcal{K}}$ to output energy level alphabet $\mathcal{M}^{\mathcal{K}}$. The probability of receiving energy level j under tag input combination i is[7]

$$P(\bar{z}_j \mid \bar{c}_i) = P(z \in \mathcal{R}_j \mid \mathcal{H}_i) = \int_{\mathcal{R}_j} f(z \mid \mathcal{H}_i) \mathrm{d}z. \quad (12)$$

On top of this, we can compute the marginal probability on all tags and obtain K transition matrices from $\mathcal{M}$ to $\mathcal{M}^{\mathcal{K}}$ that compose a discrete memoryless MAC. The probability of observing energy level j when tag k at status m_k is

$$P(\bar{z}_j \mid \bar{c}_{m_k}) = \frac{\sum_{m_{\mathcal{K}\setminus k}} P(\bar{z}_j \mid \bar{c}_{m_{\mathcal{K}}})}{\sum_{m_{\mathcal{K}}} P(\bar{z}_j \mid \bar{c}_{m_{\mathcal{K}}})}. \quad (13)$$

In summary, with CSI knowledge and for any given precoder and detection threshold set, we can obtain the expected power of the received signal per block by (6), the conditional probability density function of the accumulated energy by (7), the decision region by (8), the equivalent point-to-point channel by (12), and the discrete memoryless MAC by (13).

C. Backscatter sum-rate

Before investigating the sum-rate of the tags, we introduce some prerequisites of information theory. Define the input probability distribution of tag k at status m_k as $P_k(\bar{c}_{m_k})$, and assume the input distribution of all tags are mutually independent, i.e., $P_{\mathcal{K}}(\bar{c}_{m_{\mathcal{K}}}) = \prod_{k \in \mathcal{K}} P_k(\bar{c}_{m_k})$. Following [13], the backscatter information function associated with tag input combination $\bar{c}_{m_{\mathcal{K}}}$ is defined as

$$I_{\mathrm{B}}(\bar{c}_{m_{\mathcal{K}}}; z) \triangleq \sum_j P(\bar{z}_j \mid \bar{c}_{m_{\mathcal{K}}}) \log \frac{P(\bar{z}_j \mid \bar{c}_{m_{\mathcal{K}}})}{P(\bar{z}_j)}, \quad (14)$$

the marginal information function on $\mathcal{S} \subset \mathcal{K}$ is written as

$$I_{\mathrm{B},\mathcal{S}}(\bar{c}_{m_{\mathcal{S}}}; z) = \sum_{m_{\mathcal{K}\setminus\mathcal{S}}} P_{\mathcal{K}\setminus\mathcal{S}}(\bar{c}_{m_{\mathcal{K}\setminus\mathcal{S}}}) I(\bar{c}_{m_{\mathcal{K}}}; z), \quad (15)$$

and the mutual information of the tags and the received signal can be expressed as[8]

$$I_{\mathrm{B}}(c_{\mathcal{K}}; z) = \mathbb{E}_{c_{\mathcal{K}}}\left[I_{\mathrm{B}}(\bar{c}_{m_{\mathcal{K}}}; z)\right] = \mathbb{E}_{c_{\mathcal{S}}}\left[I_{\mathrm{B},\mathcal{S}}(\bar{c}_{m_{\mathcal{S}}}; z)\right]. \quad (16)$$

Evidently, for a given discrete memoryless MAC with transition probability $P(z \mid c_{\mathcal{K}})$, the information function $I(\bar{c}_{m_{\mathcal{K}}}; z)$ and mutual information $I(c_{\mathcal{K}}; z)$ only depend on the tag input distribution $P_k(\bar{c}_{m_k})$, $\forall m_k \in \mathcal{M}$, $\forall k \in \mathcal{K}$. Therefore, the mutual information of the tags can be explicitly written as

$$I_{\mathrm{B}}(c_{\mathcal{K}}; z) = \sum_{m_{\mathcal{K}}} \prod_{k \in \mathcal{K}} P_k(\bar{c}_{m_k}) \sum_j P(\bar{z}_j \mid \bar{c}_{m_{\mathcal{K}}}) \log \frac{P(\bar{z}_j \mid \bar{c}_{m_{\mathcal{K}}})}{P(\bar{z}_j)}. \quad (17)$$

D. Primary ergodic rate

Once the tag symbol set $\bar{c}_{m_{\mathcal{K}}}$ is successfully decoded, the user can eliminate the backscatter uncertainty and model it within the equivalent primary channel by (5). For primary transmission, the tags adjust the propagation environment in a potentially beneficial manner, and create artificial channel variation within each fading block. As such, the ergodic primary mutual information can be expressed as

$$\begin{aligned} I_{\mathrm{P}} &= \mathbb{E}_{c_{\mathcal{K}}}\left[\log_2\left(1 + \frac{|\boldsymbol{h}_{\mathrm{E}}^H(c_{\mathcal{K}})\boldsymbol{w}|^2}{\sigma_w^2}\right)\right] \\ &= \sum_{m_{\mathcal{K}}} \prod_{k \in \mathcal{K}} P_k(\bar{c}_{m_k}) \log_2\left(1 + \frac{|\boldsymbol{h}_{\mathrm{E}}^H(\bar{c}_{m_{\mathcal{K}}})\boldsymbol{w}|^2}{\sigma_w^2}\right) \text{ [bps/Hz]}. \end{aligned} \quad (18)$$

which is also a function of the tag input distribution $P(c_{\mathcal{K}})$.

III. Input Distribution, Decision Region, and Precoder Design

A. Primary ergodic-secondary sum rate region

To achieve a flexible tradeoff between the primary and backscatter links, we aim to optimize the tag input distribution, decision region, and precoder to maximize the weighted sum of the ergodic primary rate and the total backscatter rate, under the average transmit power and probability constraints

$$\max_{P(c_{\mathcal{K}}), \mathcal{T}, \boldsymbol{w}} \quad I \triangleq \rho I^{\mathrm{P}} + (1-\rho) I^{\mathrm{B}} \quad (19a)$$

$$\text{s.t.} \quad \|\boldsymbol{w}\|^2 \leq P, \quad (19b)$$

$$\sum_{m_k} P_k(\bar{c}_{m_k}) = 1, \quad \forall k \in \mathcal{K}, \quad (19c)$$

$$P_k(\bar{c}_{m_k}) \geq 0, \quad \forall m_k \in \mathcal{M}, \ \forall k \in \mathcal{K} \quad (19d)$$

where $\rho \in [0, 1]$ denotes the priority of the primary link. As problem (19) is not jointly convex over $P(c_{\mathcal{K}})$, $\mathcal{T}$ and $\boldsymbol{w}$, we propose an Block Coordinate Descent (BCD)-based algorithm that iteratively updates the input distribution, decision region, and precoder, until convergence.

[7]For simplicity, we assume there exists at least one feasible precoder that produces distinct received energy levels for all tag input combinations. [TODO] Merge with precoder design.

[8]Please be aware that $c_{\mathcal{K}}$, $c_{\mathcal{S}}$, z are random variables, while $\bar{c}_{m_{\mathcal{K}}}$ (and $\bar{c}_i$), $\bar{c}_{m_{\mathcal{S}}}$, $\bar{z}_j$ represent the corresponding instances.

B. Input distribution

Once the decision boundaries $\mathcal{T}$ and the precoder $\boldsymbol{w}$ are determined, obtain the equivalent discrete memoryless MAC by (13). The input distribution optimization subproblem is

$$\max_{P(c_{\mathcal{K}})} \quad I \tag{20a}$$

$$\text{s.t.} \quad \sum_{m_k} P_k(\bar{c}_{m_k}) = 1, \quad \forall k \in \mathcal{K}, \tag{20b}$$

$$P_k(\bar{c}_{m_k}) \geq 0, \quad \forall m_k \in \mathcal{M}, \ \forall k \in \mathcal{K} \tag{20c}$$

Although the domain is non-convex for $K > 1$, the Karush–Kuhn–Tucker (KKT) conditions are sufficient and necessary for an input distribution to achieve the weighted sum-capacity. The proof follows straightforwardly from [14] and details are omitted here.[9]

C. Decision region

As indicated by [15], the optimal ML decision regions are very close to the optimal decision regions to problem (19). We can either use (8) as suboptimal, or take derivative of (16) w.r.t. $T_{i-1,i}$ and $T_{i,i+1}$ (however, closed-form solutions are unavailable and two-dimensional search is needed).

D. Precoder

Interestingly, we can design precoder to adjust the expectation of the received power (6) at each tag input combination, which can avoid the detection blind spots in [11] and further boost the weighted sum-rate. However, the problem is highly non-convex – the information function associated with input combination status i is

$$I(\bar{c}_i; z) = \sum_{j \in \mathcal{M}^{\mathcal{K}}} \int_{T_{j-1,j}}^{T_{j,j+1}} \frac{z^{N-1} \exp\left(-\frac{z}{\mathrm{tr}(H_{\mathrm{E},i}W)+\sigma_w^2}\right)}{\left(\mathrm{tr}(H_{\mathrm{E},i}W)+\sigma_w^2\right)^N (N-1)!} \mathrm{d}z \times \log \frac{\int_{T_{j-1,j}}^{T_{j,j+1}} \frac{z^{N-1} \exp\left(-\frac{z}{\mathrm{tr}(H_{\mathrm{E},i}W)+\sigma_w^2}\right)}{\left(\mathrm{tr}(H_{\mathrm{E},i}W)+\sigma_w^2\right)^N (N-1)!} \mathrm{d}z}{\sum_{i' \in \mathcal{M}^{\mathcal{K}}} \int_{T_{j-1,j}}^{T_{j,j+1}} \frac{z^{N-1} \exp\left(-\frac{z}{\mathrm{tr}(H_{\mathrm{E},i'}W)+\sigma_w^2}\right)}{\left(\mathrm{tr}(H_{\mathrm{E},i'}W)+\sigma_w^2\right)^N (N-1)!} \mathrm{d}z}, \tag{21}$$

and the mutual information can be expressed as a function of W by combining (16) and (21).

So far I have no idea how to solve this issue, and found no reference regarding precoder design for AmBC/SR with discrete channels (although some naive combiner designs are available for BIBO). Personally, I believe the precoder design is the key to (i) boost the rate region and avoid blind spots in conventional AmBC; (ii) build our proposal over existing infrastructures. Ideally, assuming the number of transmit antennas Q is larger than the number of tags K, the optimal energy levels should be almost uniformly spaced (as z follows Erlang distribution) to concentrate the channel transitional probability on diagonal as possible.

[9] For any elementary MAC (the sizes of input alphabets are no greater than that of the output alphabet), the sufficiency can be proved by local maximum and connectedness of KKT solutions. Also, the capacity of an arbitrary MAC is achieved by an elementary MAC included within.

References

[1] J. Kim and B. Clerckx, "Wireless Information and Power Transfer for IoT: Pulse Position Modulation, Integrated Receiver, and Experimental Validation," *arXiv:2104.08404*, pp. 1–15, apr 2021. [Online]. Available: http://arxiv.org/abs/2104.08404

[2] R. Hansen, "Relationships Between Antennas as Scatterers and as Radiators," *Proceedings of the IEEE*, vol. 77, no. 5, pp. 659–662, may 1989. [Online]. Available: http://ieeexplore.ieee.org/document/32056/

[3] C. Boyer and S. Roy, "Backscatter Communication and RFID: Coding, Energy, and MIMO Analysis," *IEEE Transactions on Communications*, vol. 62, no. 3, pp. 770–785, mar 2014. [Online]. Available: http://ieeexplore.ieee.org/document/6685977/

[4] Daniel Dobkin, *The RF in RFID: Passive UHF RFID in Practice*. London, U.K.: Newnes, nov 2012. [Online]. Available: https://www.elsevier.com/books/the-rf-in-rfid/dobkin/978-0-12-394583-9

[5] S. J. Thomas, E. Wheeler, J. Teizer, and M. S. Reynolds, "Quadrature Amplitude Modulated Backscatter in Passive and Semipassive UHF RFID Systems," *IEEE Transactions on Microwave Theory and Techniques*, vol. 60, no. 4, pp. 1175–1182, apr 2012. [Online]. Available: http://ieeexplore.ieee.org/document/6153042/

[6] D. Bharadia, K. R. Joshi, M. Kotaru, and S. Katti, "BackFi: High Throughput WiFi Backscatter," in *Proceedings of the 2015 ACM Conference on Special Interest Group on Data Communication*, vol. 45, no. 4. New York, NY, USA: ACM, aug 2015, pp. 283–296. [Online]. Available: https://dl.acm.org/doi/10.1145/2785956.2787490

[7] G. Yang, C. K. Ho, and Y. L. Guan, "Multi-Antenna Wireless Energy Transfer for Backscatter Communication Systems," *IEEE Journal on Selected Areas in Communications*, vol. 33, no. 12, pp. 2974–2987, dec 2015. [Online]. Available: http://ieeexplore.ieee.org/document/7274644/

[8] H. Guo, Q. Zhang, S. Xiao, and Y.-C. Liang, "Exploiting Multiple Antennas for Cognitive Ambient Backscatter Communication," *IEEE Internet of Things Journal*, vol. 6, no. 1, pp. 765–775, feb 2019. [Online]. Available: https://ieeexplore.ieee.org/document/8411483/

[9] Q. Wu and R. Zhang, "Intelligent Reflecting Surface Enhanced Wireless Network via Joint Active and Passive Beamforming," *IEEE Transactions on Wireless Communications*, vol. 18, no. 11, pp. 5394–5409, nov 2019. [Online]. Available: https://ieeexplore.ieee.org/document/8811733/

[10] H. Guo, Y.-C. Liang, R. Long, and Q. Zhang, "Cooperative Ambient Backscatter System: A Symbiotic Radio Paradigm for Passive IoT," *IEEE Wireless Communications Letters*, vol. 8, no. 4, pp. 1191–1194, aug 2019. [Online]. Available: https://ieeexplore.ieee.org/document/8692391/

[11] J. Qian, A. N. Parks, J. R. Smith, F. Gao, and S. Jin, "IoT Communications With M-PSK Modulated Ambient Backscatter: Algorithm, Analysis, and Implementation," *IEEE Internet of Things Journal*, vol. 6, no. 1, pp. 844–855, feb 2019. [Online]. Available: https://ieeexplore.ieee.org/document/8423609/

[12] T. Nguyen, Y.-J. Chu, and T. Nguyen, "On the Capacities of Discrete Memoryless Thresholding Channels," in *2018 IEEE 87th Vehicular Technology Conference (VTC Spring)*, vol. 2018-June. IEEE, jun 2018, pp. 1–5. [Online]. Available: https://ieeexplore.ieee.org/document/8417506/

[13] M. Rezaeian and A. Grant, "Computation of Total Capacity for Discrete Memoryless Multiple-Access Channels," *IEEE Transactions on Information Theory*, vol. 50, no. 11, pp. 2779–2784, nov 2004. [Online]. Available: http://ieeexplore.ieee.org/document/1347364/

[14] Y. Watanabe and K. Kamoi, "A Formulation of the Channel Capacity of Multiple-Access Channel," *IEEE Transactions on Information Theory*, vol. 55, no. 5, pp. 2083–2096, may 2009. [Online]. Available: http://ieeexplore.ieee.org/document/4839058/

[15] J. Qian, Y. Zhu, C. He, F. Gao, and S. Jin, "Achievable Rate and Capacity Analysis for Ambient Backscatter Communications," *IEEE Transactions on Communications*, vol. 67, no. 9, pp. 6299–6310, sep 2019. [Online]. Available: https://ieeexplore.ieee.org/document/8721108/